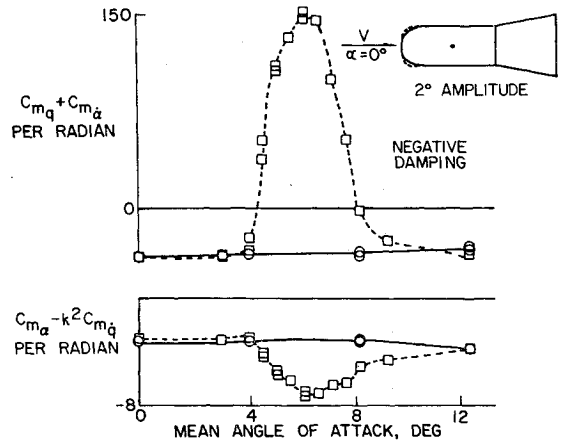

Fig. 2 Effect of nose shape on dynamic-stability parameters of a proposed re-entry vehicle.

ing and stability parameters. For the rounded-nose model, indicated by the solid lines both in the sketch and fairing of the data, both damping and stability are positive and almost constant with angle of attack. The model with a slightly more blunt nose has a region of negative damping and increased stability near 6° angle of attack due to flow separation from the upper surface of the model. Although acceptable stability parameters exist near 0° for both configurations, the negative damping near 6° for the more blunt-nose configuration indicates a possible stability problem if the body approaches 6°. Flight tests did show dynamic instability for the more blunt-nose configuration and indicated, as do these small-amplitude forced-oscillation data, that the less blunt configuration is to be preferred from the dynamic-stability point of view.

The data of Fig. 3 show some rather unexpected results of changing the shape of a body of revolution in a region of completely separated flow. For the model with a flat base, there was observed both positive damping and stability through the angle-of-attack range. With the addition of a truncated-cone fairing cap to the base of the model, in a region where the flow would certainly be completely separated, the model exhibits negative damping over a wide range of angle of attack. Free-flight tests of a similar configuration show that the addition of the base did indeed lead to dynamic instability.

An example of some small-amplitude data that have been applied to the prediction of large-amplitude motion is given in Fig. 4. These data were obtained at an oscillation amplitude of 2° over a range of angle of attack for a simple body of revolution that, when given freedom in pitch, had been observed to perform a large-amplitude limit-cycle oscillation. When these small-amplitude forced-oscillation data were used in a single-degree-of-freedom analog-computer program,

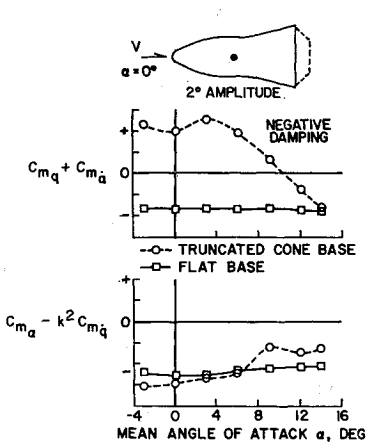

Fig. 3 Effect of base shape on dynamic-stability parameters of a proposed re-entry vehicle.

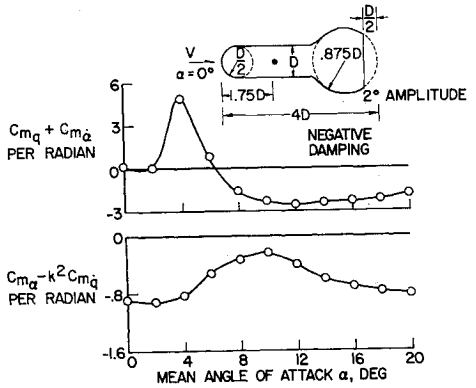

Fig. 4 Dynamic-stability parameters of a research model.

a quantitative prediction of an amplitude of 15° was obtained, compared with an observed amplitude of 13.5°. A predicted frequency of 6.8 cps was obtained, compared with an observed frequency of 7 cps.

In summary, the small-amplitude forced-oscillation technique now being used at the NASA Langley Research Center provides an accurate and convenient method of measuring some of the important dynamic-stability parameters. The small-amplitude data may be used both in the development of an acceptable configuration and in the accurate prediction of large-amplitude motion.

Reference

[1] Braslow, A. L., Wiley, H. G., and Lee, C. Q., "A rigidly forced oscillation system for measuring dynamic-stability parameters in transonic and supersonic wind tunnels," NASA TN D-1231 (1962).

Supplementary Note on Effect of Wing Geometry on Volume and Weight

B. Saelman*
Lockheed Aircraft Corporation, Burbank, Calif.

Nomenclature

W_{BB} = weight of box beam, lb
ρ = material density, lb/in.^{3}
p = pressure, lb/in.^{2}
C_R = root chord, in.
h_R = maximum root thickness, in.
f = effective stress, lb/in.^{2}
λ = taper ratio
k_{ib} = bending integration factor (see Ref. 1)
AR = aspect ratio
b = wing span, in.
S = wing area, in.^{2}
n = load factor
ϕ = box chord/wing chord
r = average box height/max box height
W = gross weight, lb
V = box beam volume, in.^{3}
θ = angle of twist, rad
T = torque, in.-lb
G = modulus of rigidity, lb/in.^{2}
J = torsion constant, in.^{4}
s = box beam perimeter, in.
t = box beam skin thickness, in.

IN the optimization procedure discussed in Ref 1 a more useful expression for wing weight may be obtained in terms of the parameters of wing area and aspect ratio. Since

Received April 17, 1964; revision received June 15, 1964.
* Design Specialist, Lockheed-California Division.

the volume is expressed in terms of these parameters in Eq. (6) of Ref 1, it would be desirable to also utilize these variables in the expression for weight.

Combining Eqs. (7) and (8) of Ref 1

$$W_{BB} = \frac{\rho p b^3 C_R}{6 h_R f}\left[\frac{\lambda}{8} + \frac{(1-\lambda)}{24}\right] k_{ib} \tag{1}$$

Substituting

$$b^2 = ARS \tag{2}$$

$$p = Wn/S \tag{3}$$

into Eq. (1),

$$W_{BB} = \frac{WnAR^{3/2}S^{1/2}\rho}{6(h_R/C_R)f}\left[\frac{\lambda}{8} + \frac{(1-\lambda)}{24}\right] k_{ib} \tag{4}$$

Now, if variations in wing weight under constant performance conditions are being considered, the wing loading, as given by Eq. (3), will be constant, and under another performance requirement the aspect ratio may be constant; we have

$$W_{BB} = \frac{\rho K A R^{3/2} S^{3/2}}{6(h_R/C_R)f}\left[\frac{\lambda}{8} + \frac{(1-\lambda)}{24}\right] k_{ib} \tag{5}$$

$$W/S = K$$

or

$$W_{BB} = \frac{\rho A R^{3/2} W^{3/2}}{6(h_R/C_R) f K^{1/2}}\left[\frac{\lambda}{8} + \frac{(1-\lambda)}{24}\right] k_{ib} \tag{6}$$

The total wing weight can be expressed as

$$W_w = W_{BB} + K_1 S \tag{6a}$$

where the secondary structure weight is shown to be proportional to wing area. The volume, given by Eq. (6) of Ref 1, may be expressed in terms of gross weight:

$$\frac{K^{3/2} V A R^{1/2}}{W^{3/2}} = \frac{0.67 r\phi}{(1+\lambda)^2}\left\{\lambda^2 (t/c)_t + (t/c)_R + \lambda[(t/c)_t (t/c)_R]^{1/2}\right\} \tag{7}$$

and the wing weight may be expressed in terms of the volume:

$$W_{BB} = \frac{K\rho A R^2 (1+\lambda)^2\{(\lambda/8) + [(1-\lambda)/24]\} k_{ib} V}{4(h_R/c_R) f r\phi\{\lambda^2 (t/c)_t + (t/c)_R + \lambda[(t/c)_t (t/c)_R]^{1/2}\}} \tag{8}$$

Equation (8) shows how wing weight varies with wing volume when performance requires wing loading and aspect ratio to remain constant. As a refinement, it is noted that the stress f is independent of chord loading for tension loadings, such as is the case for the wing lower surface where a stress level is specified for fatigue requirements; but it is to be recognized that the stress will vary with chord loading when compressive stresses are critical.

Now, considering box beams that are critical for torsional stiffness requirements, we can write

$$\theta = \int_0^{b/2} \frac{T dy}{GJ} \tag{9}$$

$$W_{BB} = \int_0^{b/2} st dy \tag{10}$$

For wings of moderate or large aspect ratios it can be shown that

$$W_{BB} \propto \frac{AR^2}{(h/c)^2} \tag{11}$$

As an example, for a constant wing geometry and constant torque,

$$\theta = T b_s / 8 G A^2 t \tag{12}$$

and

$$W_{BB} = s\left[\frac{T b_s}{8 G \theta A^2}\right]\frac{b}{2} = \frac{1}{4G\theta}\left(\frac{b}{c}\right)^2\left(\frac{c+h}{h}\right)^2 = \frac{1}{4G\theta} AR_{\text{BOX}}^2 \frac{(1+h/c)^2}{(h/c_{\text{BOX}})^2} \tag{13}$$

Letting

$$(h/c)_{\text{BOX}} = K_1 (h/c)_{\text{WING}} \qquad AR_{\text{BOX}} = K_2 (h/c)_{\text{WING}}$$

Eq. (12) can be written as

$$W_{BB} = \frac{K_2^2 AR_{\text{WING}}^2}{4G\theta K_1^2}\frac{(1+h/c)^2}{(h/c_{\text{WING}})^2} \tag{14}$$

which is of the form given by Eq. (11).

For low-aspect ratio wings in which warpage restraints are more severe, a somewhat different analysis would be required in order to obtain the relationship for stiffness critical wings.

Reference

[1] Saelman, B., "Effect of wing geometry on volume and weight," J. Aerospace Sci. 29, 1390–1392 (1962).

Design of the Bubbler Ozone Detector

M. Griggs*
General Dynamics/Astronautics, San Diego, Calif.

Introduction

It has long been desirable to have a simple and cheap method for measuring the vertical distribution of atmospheric ozone. If this is measured on a widespread regular basis, using the quasi-conservative property of ozone in the lower stratosphere, the results will be of considerable value in understanding the dynamic processes in the atmosphere. This led to the development of the bubbler ozonesonde. It is simple in design and use, gives an absolute measurement of ozone, and is cheap to produce. It has been used on many balloon flights in different parts of the world. A laboratory model has been built, but this description is limited to the balloon-borne detector.

Principle of the Bubbler

The method of detecting the ozone relies on the familiar reaction of ozone with potassium iodide solution to form free iodine. This iodine is measured by the passage of a current between two electrodes, one platinum, the other silver, immersed in the solution. The cell has a spontaneous emf that is balanced by an applied emf of about 0.43 v.

The air and ozone are bubbled through the solution, and the ozone is removed according to the equation

$$2KI + O_3 + H_2O \rightarrow 2KOH + I_2 + O_2 \tag{1}$$

Presented as Preprint 64-321 at the AIAA 1st Annual Meeting, Washington, D. C., June 29–July 2, 1964; revision received August 6, 1964. The development of this instrument was done at the Clarendon Laboratory, Oxford, England, under a grant from the Gassiot Committee of the Royal Society. The author would like to thank A. W. Brewer, now at Toronto University, for advice and encouragement in this work.

* Staff Scientist, Space Science Laboratory.